AD NUMBER

AD818285

NEW LIMITATION CHANGE

TO

Approved for public release, distribution unlimited

FROM

Distribution authorized to U.S. Gov't. agencies and their contractors; Critical Technology; JUL 1967. Other requests shall be referred to Commanding Officer, Edgewood Arsenal, Attn: SMUEA-TSTI-T, Edgewood Arsenal, MD 21010.

AUTHORITY

USAEA ltr, 14 Sep 1971

SRI Technical Report No. 9

ULTRASONIC DISSEMINATION OF AEROSOLS

Special Report

by

C. W. SMITH
C. M. ABLOW
S. V. HANAGUD
E. M. SPURLOCK
D. R. GRINE

JULY 1967

Physical Research Laboratory
Research Laboratories
Edgewood Arsenal, Maryland 21010

Contract DA-18-035-AMC-122(A)

STANFORD RESEARCH INSTITUTE
Menlo Park, California

Distribution Statement

This document is subject to special export controls and each transmittal to foreign governments or foreign nationals may be made only with prior approval of the CO, Edgewood Arsenal, ATTN: SMUEA-TSTI-T, Edgewood Arsenal, Maryland, 21010.

Disclaimer

The findings in this report are not to be construed as an official Department of the Army position unless so designated by other authorized documents.

Disposition

Destroy this report when no longer needed. Do not return it to the originator.

SRI Technical Report No. 9

ULTRASONIC DISSEMINATION OF AEROSOLS

Special Report

by

C. W. SMITH
C. M. ABLOW
S. V. HANAGUD
E. M. SPURLOCK
D. R. GRINE

July 1967

Physical Research Laboratory
Research Laboratories
Edgewood Arsenal, Maryland 21010

Contract DA-18-035-AMC-122(A)
Task 1B522301A08101
SRI Project PAU-4900

STANFORD RESEARCH INSTITUTE
Menlo Park, California

FOREWORD

The work described in this report was authorized under Task 1B522301AC8101, Dissemination Investigations of Liquid and Solid Agents (U). The work was started in April 1964 and completed in September 1966.

The information in this document has not been cleared for release to the general public.

DIGEST

An investigation of the generation of aerosol by ultrasonic means was started. Although the work was terminated before it could be completed, the methods and results of this report should be useful in any future study. The theory of a liquid flow over the surface of an oscillating reed was studied to help the understanding of high flow-rate devices. A simple resonance theory has been developed which contrasts with the usual parametric capillary wave theory. An experimental photo-optical technique has been devised and used to give quantitative information on droplet size and velocity distributions. Capillary wave behavior has been examined experimentally and compared with existing theory. A possible explanation of the transition of capillary waves to an aerosol has been suggested. The existence of cavitation during sonic aerosol production from water was verified.

CONTENTS

ILLUSTRATIONS

TABLES

I INTRODUCTION

This report summarizes a study of the problem of the basic mechanism of sonic aerosol formation.

Aerosol production from a thin liquid layer on a vibrating surface has been known for many years, yet the basic mechanism controlling the drop formation is not known with certainty. Two possibilities are generally suggested. One is that capillary waves, excited on the surface, grow to an unstable size and throw off droplets from the peaks of the waves. The theory of capillary waves themselves is well established—see for example, Eisenmenger[1]—but the step from capillary waves to aerosols has only been explained in an empirical fashion.

The other possibility is the mechanism of cavitation. The generation and collapse of microbubbles by intense sonic forces is believed to cause enough agitation in the liquid layer to cause the disruption of the surface.

A theoretical determination of capillary wave forms in a liquid layer flowing over an oscillating reed, a simple model for the high-flow devices, is made in Section II. The free surface wave is found to grow through resonant instability. In this linearized model, pressure extremes occur at the free surface (where they are balanced by inertial and surface tension forces). It follows that the cavitation mechanism for aerosol formation would be initiated near the free surface. Some correlation between aerosol drop size and capillary wave lengths is obtained.

Section III describes work, largely experimental, from another direction. Here, the approach was to first make experimental observations and then compare observations with existing theory. Work was pursued on the velocity and size distribution of the droplets. Capillary waves and the subsequent transitions to an aerosol were examined extensively. An attempt was made to obtain some design information on high flow-rate atomizers that were developed in the earlier phases of the project. Also a sampling technique was adapted for use with these high-flow devices.

Section IV is a brief summary of this work and its conclusions. Section V contains an evaluation of the preliminary results of this work and suggestions for using sonic generators for dissemination of CW agents.

The sonic studies described in this report were done by various staff members working along lines that could be separated at the beginning of the study but were to be merged as the work progressed. Because of a change in the overall SRI aerosol dissemination program, the several pieces of this study could not be completed and integrated; hence, an unavoidable lack of continuity between and within sections will be apparent to the reader.

II THEORETICAL STUDIES OF ULTRASONIC ATOMIZATION

A. Capillary Waves Formed on the Surface of Fluid Flowing over an Oscillating Surface

This theoretical study has the objective of determining the wave length of small capillary waves on the surface of fluid flowing over an oscillating surface. The wave length is of interest since it is likely to be closely related to droplet diameter of any aerosol produced from the fluid.,

The analysis begins with an idealization of the physical situation. The present mathematical model differs in two ways from those used in previously published analyses.[2,3]

(1) The oscillator is considered to have a rocking motion rather than a uniform transverse vibration. This complicates the analysis, since the underlying smooth flow fitting the oscillating boundary is no longer just a rigid motion of the fluid. The rocking motion more closely simulates the motion of our high-flow devices (Section III-A-4).

(2) The amplitude of the waves is supposed to be comparable to the amplitude of the excitation. This is likely to be the case near the upper limit of validity of a linearized, small-wave theory.

The results differ from previous results in that the unstable waves are of resonant rather than of the parametrically excited type. They are simple standing sine waves and so fail to explain the observed localization of unstable waves on the disseminator.

1. Mathematical Model

In the model, the oscillating surface is taken to be infinitely wide and its mode of oscillation is simplified to that of a rigid, flat plane in oscillatory rotation through a small angle about a fixed axis.

The fluid is supposed to be inviscid and incompressible and to be in irrotational, two-dimensional motion. It follows that there is a velocity potential Φ obeying Laplace's equation

$$\Phi_{XX} + \Phi_{YY} = 0 \tag{1}$$

such that the velocity components are Φ_X and Φ_Y. Here (X,Y) are laboratory coordinates, and literal subscripts indicate partial differentiation.

Bernoulli's law[4] relates the pressure P to the potential function:

$$P/\rho + (\Phi_X^2 + \Phi_Y^2)/2 + \Phi_T = C(T) \tag{2}$$

where ρ is the constant density, T is the time, and C is an arbitrary function of T alone. If $F(X,Y,T) = 0$ is a surface along which the fluid particles flow, *i.e.*, a material surface in the fluid, the kinematic condition relating F and Φ reads

$$F_T + \Phi_X F_X + \Phi_Y F_Y = 0 \quad . \tag{3}$$

For the function F defining the free surface, (2) and (3) hold with the pressure in (2) being due to surface tension and therefore taken proportional to the curvature K of the free surface:

$$K = (F_{XX}F_Y^2 - 2F_{XY}F_XF_Y + F_{YY}F_X^2)/(F_X^2 + F_Y^2)^{3/2} \quad . \tag{4}$$

If the constant of proportionality is written ρT_0 the free surface dynamic condition becomes

$$\Phi_T + (\Phi_X^2 + \Phi_Y^2)/2 = T_0 K \quad . \tag{5}$$

To complete the model, the wall oscillations and conditions need to be specified up- and down-stream of the region of interest. To obtain a first, simplest problem, take the wall to be straight and rotating:

$$Y = X \tan \Theta, \quad \Theta = A \sin \omega T \tag{6}$$

where A and ω are given positive constants, $A < \pi/2$. The region of interest is $0 \le X \le L$, $Y > 0$.

Conditions at $X = 0$ and $X = L$ are specified below to simplify the mathematics.

2. Boundary-Fitting Coordinates

It is convenient to introduce coordinates (x,y,t) in place of (X,Y,T) by means of

$$\begin{aligned} x &= (X\cos\Theta + Y\sin\Theta)/L \\ y &= (-X\sin\Theta + Y\cos\Theta)/L \\ t &= \omega T \end{aligned} \tag{7}$$

where the length L of the reed and the circular frequency ω of its oscillation have been used for the nondimensionalization. Potential function Φ and surface function F are replaced by

$$\begin{aligned} \phi(x,y,t) &= [\Phi(X,Y,T) - \int_0^T C(T)dT]/\omega L^2 \\ f(x,y,t) &= F(X,Y,T) \quad . \end{aligned} \tag{8}$$

One finds that ϕ satisfies Laplace's equation in the new coordinates:

$$\phi_{xx} + \phi_{yy} = 0 \quad . \tag{9}$$

The kinematic condition on any material surface $f(x,y,t) = 0$ reads

$$f_t + (yf_x - xf_y)A\dot{\Theta}' + \phi_x f_x + \phi_y f_y = 0 \quad \text{on} \quad f = 0 \quad . \tag{10}$$

If $f = 0$ is the free surface, dynamic condition (5) becomes

$$\varphi_t + (y\phi_x - x\phi_y)A\dot{\Theta}' + (\phi_x^2 + \phi_y^2)/2 + T_1(f_{xx}f_y^2 - 2f_{xy}f_xf_y + f_{yy}f_x^2)/(f_x^2 + f_y^2)^{3/2} = 0$$
$$\text{on} \quad f = 0 \tag{11}$$

where

$$\theta = \sin t, \quad T_1 = T_0/\omega^2 L^3 \qquad (12)$$

and the prime indicates differentiation for a function with one argument.

The kinemati. condition on the oscillating wall is found by putting $f \equiv y$ in equation (10):

$$\phi_y = xA\theta' \quad \text{on} \quad y = 0 \quad . \qquad (13)$$

The two conditions on the free surface are simplified if function f is considered to be solved for y so that $f = y - g(x,t)$. These conditions then read

$$g_t + (yA\theta' + \phi_x)g_x + xA\theta' - \phi_y = 0 \qquad \text{on} \quad y = g \qquad (14)$$

$$\phi_t + (y\phi_x - x\phi_y)A\theta' + (\phi_x^2 + \phi_y^2)/2 = T_1 g_{xx}/(1 + g_x^2)^{3/2} \qquad \text{on} \quad y = g \quad . \qquad (15)$$

Upstream and downstream boundary conditions are prescribed somewhat arbitrarily. A simple requirement is that the flow in the y direction is the same as that of the vibrating reed at both places:

$$\phi_y = 0 \qquad \text{at} \quad x = 0 \qquad (16)$$

$$\phi_y = A\theta' \qquad \text{at} \quad x = 1 \quad . \qquad (17)$$

3. Perturbation Series

Parameter A is small and serves as a perturbation parameter. When $A = 0$ there is no flow, so that potential function ϕ can be taken to be zero, and free surface height g to be a constant, h. Assuming that ϕ and g can be expressed as series in A gives

$$\phi = A\phi^{(1)} + A^2\phi^{(2)} + \ldots$$

$$g = h + Ag^{(1)} + A^2 g^{(2)} + \ldots \qquad (18)$$

where the coefficients of powers of A are functions of x, y, and t. Substitution of the series into the various equations shows that the $\phi^{(i)}$ are all solutions of Laplace's equation.

From equations (13), (16), and (17)

$$\left.\begin{aligned} \phi_y^{(1)} &= x\theta' \\ \phi_y^{(i)} &= 0 \quad i = 2, 3, \ldots \end{aligned}\right\} \quad \text{on } y = 0 \text{ or } x = 0 \text{ or } x = 1 \quad . \tag{19}$$

Equation (14) gives, through terms in A^2,

$$g_t^{(1)} + x\theta' - \phi_y^{(1)} = 0 \quad \text{on} \quad y = h \tag{20}$$

$$g_t^{(2)} + h\theta' g_x^{(1)} + \phi_x^{(1)} g_x^{(1)} - \phi_{yy}^{(1)} g^{(1)} - \phi_y^{(2)} = 0 \quad \text{on} \quad y = h \tag{21}$$

where ϕ_y on $y = g$ is expanded into a series in A:

$$\phi_y\big|_g = A[\phi_y^{(1)}|_h + Ag^{(1)}\phi_{yy}^{(1)}|_h + \ldots] + A^2[\phi_y^{(2)}|_h + \ldots] \quad . \tag{22}$$

Similar treatment of equation (15) gives

$$\phi_t^{(1)} = T_1 g_{xx}^{(1)} \quad \text{on} \quad y = h \tag{23}$$

$$\phi_{xy}^{(1)} g^{(1)} + \phi_t^{(2)} + [h\phi_x^{(1)} - x\phi_y^{(1)}]\theta' + \{[\phi_x^{(1)}]^2 + [\phi_y^{(1)}]^2\}/2 = T_1 g_{xx}^{(2)} \quad \text{on} \quad y = h. \tag{24}$$

4. First Order Solution Functions

The general solution of Laplace's equation which satisfies the boundary conditions prescribed for $\phi^{(1)}$ in equation (19) reads

$$\phi^{(1)} = x(y - h)\theta' + \sum_{n=1}^{\infty} B_n \sin n\pi x \cosh n\pi y \tag{25}$$

where the B_n are as yet unknown functions of t. Eliminating $g^{(1)}$ between equations (20) and (23) gives the other condition on $\phi^{(1)}$:

$$\phi_{tt}^{(1)}\big|_h = T_1 \phi_{xxy}^{(1)} \quad \text{on} \quad y = h \quad . \tag{26}$$

Substitution of the expanded form of $q^{(1)}$ gives

$$\sum_{n=1}^{\infty} \sin n\pi x \{B_n'' \cosh n\pi h + (n\pi)^3 T_1 B_n \sinh n\pi h\} = 0 \quad . \tag{27}$$

Since the functions $\sin n\pi x$ are linearly independent, their coefficients in equation (27) separately vanish:

$$B_n'' + \lambda_n^2 B_n = 0$$

$$\lambda_n^2 = (n\pi)^3 T_1 \tanh n\pi h \quad . \tag{28}$$

From this

$$B_n = B_{n0} \cos \lambda_n t + B_{n1} \sin \lambda_n t \tag{29}$$

where B_{n0} and B_{n1} are constants determined by some initial condition.

Equation (20) gives

$$g^{(1)} = \sum_{n=1}^{\infty} (n\pi/\lambda_n) \sin n\pi x \sinh n\pi h \{B_{n0} \sin \lambda_n t - B_{n1} \cos \lambda_n t\} \quad . \tag{30}$$

Assuming that at a certain time the free surface is unruffled and its particles are momentarily still implies $B_{n0} = B_{n1} = 0$ for all n so that

$$\varphi^{(1)} = x(y - h)\theta' \quad , \quad g^{(1)} = 0 \tag{31}$$

which is taken to be the first order solution.

5. Second Order Solution Functions

The equations to be satisfied by $\varphi^{(2)}$ and $g^{(2)}$ are Laplace's equation and conditions (19), (21), and (24). The last two read

$$g_t^{(2)} - \varphi_y^{(2)} = 0 \qquad \text{on} \quad y = h \tag{32}$$

$$\varphi_t^{(2)} - (x\theta')^2/2 = T_1 g_{xx}^{(2)} \qquad \text{on} \quad y = h \tag{33}$$

while the general solution of the other equations is

$$\varphi^{(2)} = \sum_{n=1}^{\infty} C_n \sin n\pi x \cosh n\pi y \quad . \tag{34}$$

Elimination of $g^{(2)}$ between equations (32) and (33) gives

$$\varphi_{tt}^{(2)} = T_1\phi_{xxy}^{(2)} + x^2\theta'\theta'' \quad \text{on} \quad y = h \quad . \tag{35}$$

The solution of this equation under quiescent initial conditions has the form of equation (34) with

$$C_n = \begin{cases} [D_n/(\lambda_n^2 - 4)] \sin 2t & , \quad \lambda_n \neq 2 \\ [-D_n/4]t \cos 2t & , \quad \lambda_n = 2 \end{cases} \tag{36}$$

where

$$D_n = \{(-1)^n[(n\pi)^2 - 2] + 2\}/(n\pi)^3 \cosh n\pi h \tag{37}$$

and λ_n is defined in equation (28).

The system is resonant at $\lambda_n = 2$. The corresponding value of n is the integer n_0 nearest to a solution of

$$(n_0\pi)^3 T_1 \tanh n_0\pi h = 4 \quad . \tag{38}$$

The wave with n_0 crests and troughs either has much greater amplitude than other waves if λ_{n0} is near to but different from 2, or it has an amplitude growing with time if $\lambda_{n0} = 2$.

In approximation one takes

$$\varphi^{(2)} = C_{n0} \sin n_0\pi x \cosh n_0\pi y \quad . \tag{39}$$

By equation (32) there corresponds

$$g^{(2)} = n_0\pi\bar{C}_{n0} \sin n_0\pi x \sinh n_0\pi y \tag{40}$$

where

$$\bar{C}_{n0} = \begin{cases} -[D_n/2(\lambda_n^2 - 4)] \cos 2t \\ -(D_n/16)(\cos 2t + 2t \sin 2t) \quad . \end{cases} \tag{41}$$

6. Aerosol Formation

One theory of aerosol formation relates droplet size directly to the wavelength of capillary surface waves. The wavelength Λ of the resonant surface wave found above is $2L/n_0$. If $n_0\pi h \ll 1$, then $\tanh n_0\pi h \doteq n_0\pi h$ and equation (38) can be solved for n_0 so that

$$\Lambda = 2\pi L(\gamma_1 h/4)^{1/4} = 2\pi(\gamma hL/4\rho\omega^2)^{1/4} \qquad (42)$$

where $\gamma = \rho T_0$ is the surface tension and hL the undisturbed depth of the fluid.

Data reported in Tables II and III in Section III-A were obtained in experiments with different fluids at nearly the same frequency. For a qualitative result, one can assume the fluid depth to have also been constant. It is then possible to calculate by means of equation (42) the dependence of droplet diameter on surface tension and fluid density. This is done by assuming wavelength and aerosol diameter to be proportional with proportionality constant given by the data for water. One finds a rough agreement with observation, as seen in Table I.

Table I

THEORETICAL DROPLET DIAMETERS

LIQUID	THEORETICAL DIAMETER (microns)	AVERAGE OBSERVED DIAMETER (microns)
Water	30	30
Acetone	24	22
Ethanol	24	19
Methylene chloride	25	30
Toluene	25	20
Ethyl acetate	23	20

In another theory, droplets are supposed to be formed during the catastrophic collapse of cavities. Equation (39) shows the potential, φ, to be proportional to $\cosh n_0\pi y$. Hence, derivatives of φ and, by equation (2), pressure variations are greatest at the free surface, where y is greatest. The present analysis thus predicts that cavitation will be concentrated near the free surface of the liquid.

7. Discussion of the Model

The mathematical model above is one in which the waves are of amplitudes comparable to that of the reed. The smooth flow on which the waves are superposed has been taken to be one in which the fluid surface remains parallel to the reed. The results of these assumptions are that the effects of rotation are minimized, and that the waves have uniform amplitude down the length of the reed. Also, the type of instability shown is just the large amplitude resonant response of a linear, fixed-parameter system driven near a critical frequency. This resonance occurs at twice the driving frequency.

By contrast, the theory of Benjamin and Ursell,[2] which is well supported by their experiments, provides instability excited parametrically. The unstable waves grow exponentially fast, their fundamental frequency is half that of the driver, and harmonics of the fundamental are also unstable.

The main difference between the two theories seems to be that the driver amplitude is small in the present theory—of similar magnitude to the resulting waves—while in the theory of Benjamin and Ursell the waves considered are small with respect to the driver amplitude. This is evident in their linearization of the Bernoulli equation, where a product of driver amplitude and wave amplitude is retained. Such a product is a term of second order here and would not survive linearization.

A major feature of the observed flow that has not been found in the present analysis is the localization of instability. The waves found here stand with constant amplitude down the length of the reed, while aerosol formation occurs only near the tip of the reed. Taking the basic smooth flow to be flow with fixed free surface instead of flow with free surface following the reed oscillations may correct this defect of the theory.

An experimental device presenting a wide flat surface undergoing simple rocking oscillations is shown in Figure 1. The waves over a large part of the aluminum wedge should be uniform and regular, with no distortion from curvature of the underlying surface or from edge effects. The theoretical analysis presented above refers directly to this configuration. This experimental device would facilitate the needed comparisons with theory.

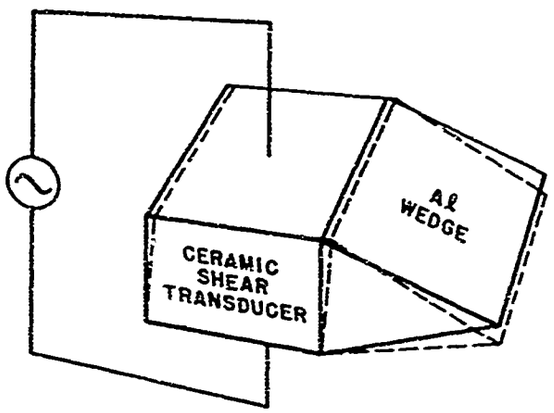

FIG. 1 A SIMPLE-GEOMETRY ULTRASONIC DISSEMINATOR

B. Determination of the Normal Modes of Vibration of the Wedge-Shaped Device

1. The Physical Model

The physical model is an axially symmetric shaft with the cross-section shown in the following figure. In view of the axial symmetry, the radial and vertical displacements, u and w respectively, will depend only on the coordinates r and z.

Suitable boundary conditions might be

$$u = 0, \frac{\partial u}{\partial z} = 0, w = 0 \quad \text{at} \quad z = 0 \tag{1}$$

$$\sigma_r = 0, \sigma_{rz} = 0 \quad \text{at} \quad r = b \tag{2}$$

and

$$\sigma_n = 0, \sigma_t = 0 \quad \text{at} \quad r = bz/l \tag{3}$$

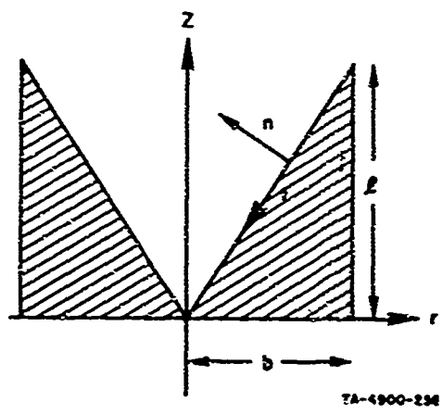

where n and t are normal and tangential directions and σ represents stress in the usual notation.

Since the nonzero stresses are given by

$$\sigma_r = \lambda\left(\frac{\partial u}{\partial r} + \frac{u}{r} + \frac{\partial w}{\partial z}\right) + 2G\frac{\partial u}{\partial r} \tag{4}$$

$$\sigma_z = \lambda\left(\frac{\partial u}{\partial r} + \frac{u}{r} + \frac{\partial w}{\partial z}\right) + 2G\frac{\partial w}{\partial z} \tag{5}$$

$$\sigma_\theta = \lambda\left(\frac{\partial u}{\partial r} + \frac{u}{r} + \frac{\partial w}{\partial z}\right) + 2G\frac{u}{r}$$

$$\sigma_{rz} = G\left(\frac{\partial w}{\partial r} + \frac{\partial u}{\partial z}\right) \tag{6}$$

where G is the modulus of rigidity, we can rewrite the boundary conditions (2) and (3) in terms of the displacements as follows :

$$(\lambda + 2G)\frac{\partial u}{\partial r} + \lambda\left(\frac{u}{r} + \frac{\partial w}{\partial z}\right) = 0 \tag{2a}$$

$$\frac{\partial w}{\partial r} + \frac{\partial u}{\partial z} = 0 \tag{2b}$$

$$\lambda(b^2 + l^2)\left(\frac{\partial u}{\partial r} + \frac{u}{r} + \frac{\partial w}{\partial z}\right) + 2G\left(l^2\frac{\partial u}{\partial r} + b^2\frac{u}{r}\right) - 2blG\left(\frac{\partial w}{\partial r} + \frac{\partial u}{\partial z}\right) = 0 \tag{3a}$$

$$(l^2 - b^2)\left(\frac{\partial w}{\partial r} + \frac{\partial u}{\partial z}\right) + 2bl\left(\frac{\partial u}{\partial r} - \frac{\partial w}{\partial z}\right) = 0 \tag{3b}$$

The proposed method of solution is that of Rayleigh-Ritz, described here briefly. Let V and T be potential and kinetic energies of the model at any time. Then V is a function of the nonzero strains.

$$\epsilon_r = \frac{\partial u}{\partial r} \tag{7}$$

$$\epsilon_\theta = \frac{u}{r} \tag{8}$$

$$\epsilon_z = \frac{\partial w}{\partial z} \tag{9}$$

$$\epsilon_{rz} = \frac{1}{2}\left(\frac{\partial w}{\partial r} + \frac{\partial u}{\partial z}\right) \tag{10}$$

while T is a function of the displacements u and w. If we suppose that u and w have the forms

$$u = \sum_{i=1}^{n} a_i u_i \tag{11}$$

$$w = \sum_{i=1}^{n} a_i w_i \tag{12}$$

where the a_i are constants and the u_i and w_i are functions of r and z, and that each pair, u_i and w_i, satisfies the boundary conditions (1), (2a), (2b), (3a) and (3b), then V and T will depend on the a_i. The ratio

$$\lambda = \frac{V_{max}}{T_{max}} \tag{13}$$

is minimized with respect to the a_i when

$$\frac{\partial}{\partial a_i} V_{max} - \lambda \frac{\partial}{\partial a_i} T_{max} = 0 \ , \ i = 1, 2, \ldots, n \ . \tag{14}$$

Equations (14) are linear and homogenous in the a_i and thus will have a nontrivial solution only when the determinant of the coefficients vanishes. This condition reduces to an nth degree polynomial equation in λ called the characteristic equation. The roots, $\lambda_i^{(n)}$ of the characteristic equation provide upper bounds for the squares of the first n natural frequencies of the model; that is,

$$\lambda_1^{(n)} \geq \omega_1^2 \ , \ \lambda_2^{(n)} \geq \omega_2^2 \ , \ \ldots, \ \lambda_n^{(n)} \geq \omega_n^2 \ . \tag{15}$$

In the case that the set of functions $\{u_1, w_1, u_2, w_2, \ldots\}$ is complete then

$$\lambda_i^{(n)} \to \omega_i^2 \quad \text{as} \quad n \to \infty \ .$$

While the method described is theoretically applicable, it appears difficult to generate a sequence (u_i, w_i) that satisfies the boundary conditions. Furthermore, there is some question regarding the proper

boundary conditions. In particular, the condition $w = 0$ of (1) may not be the wisest choice for model compatability.

2. A Numerical Case

As a simple example, the following functions were selected:

$$u = \frac{az^2}{l^2}\left(\frac{r}{b} - 1\right)^2\left(\frac{r}{b} - \frac{z}{l}\right)^2 \qquad (16)$$

$$w = -\frac{ab}{l}\left(\frac{r}{b} - 1\right)^2\left(\frac{r}{b} - \frac{z}{l}\right)^2\left(\frac{5}{6}\frac{r}{b} - \frac{1}{2} - \frac{1}{3}\frac{z}{l}\right)$$

$$= -\frac{ab}{l}\left(\frac{r}{b} - 1\right)^2\left(\frac{r}{b} - \frac{z}{l}\right)^2\left[\frac{1}{3}\left(\frac{r}{b} - \frac{z}{l}\right) + \frac{1}{2}\left(\frac{r}{b} - 1\right)\right] . \qquad (17)$$

Then V has the expression

$$V = \pi\int_{z=0}^{z=l}\int_{r=b\frac{z}{l}}^{r=b}\{\lambda(\epsilon_r + \epsilon_\theta + \epsilon_z)^2 + 2\mu(\epsilon_r^2 + \epsilon_\theta^2 + \epsilon_z^2) + \mu\epsilon_{rz}^2\}r\,dr\,dz . \qquad (18)$$

3. Change of Variables

By changing the variables

$$\bar{r} = \frac{r}{b} - 1,\ \bar{\eta} = \frac{r}{b} - \frac{z}{l},\ u(r,z) = \bar{u}(\bar{r},\bar{\eta}),\ w(r,z) = \bar{w}(\bar{r},\bar{\eta})$$

$$\bar{\epsilon}_r(\bar{r},\bar{\eta}) = \epsilon_r(r,z),\ \bar{\epsilon}_\theta(\bar{r},\bar{\eta}) = \epsilon_\theta(r,z)$$

$$\bar{\epsilon}_\eta(\bar{r},\bar{\eta}) = \epsilon_z(r,z),\ \bar{\epsilon}_{r\eta}(\bar{r},\bar{\eta}) = \epsilon_{rz}(r,z) . \qquad (19)$$

To evaluate the integral, note that region of integration over r and z is

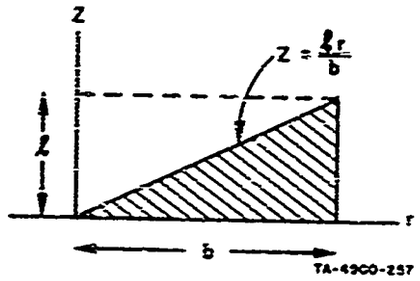

which in $\bar{r} - \bar{\eta}$ coordinates is

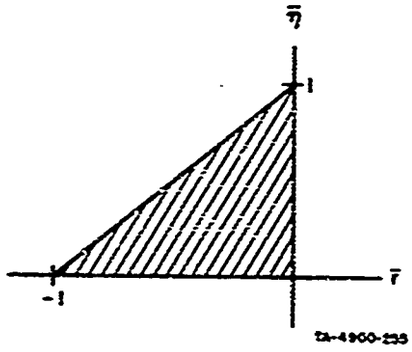

Also

$$J = \frac{\partial(r,z)}{\partial(\bar{r},\bar{\eta})} = \frac{\partial r}{\partial \bar{r}}\frac{\partial z}{\partial \bar{\eta}} - \frac{\partial r}{\partial \bar{\eta}}\frac{\partial z}{\partial \bar{r}} \qquad (20)$$

where

$r = b(1 + \bar{r})$, $z = \ell(1 + \bar{r} - \bar{\eta})$ so that

$J = -b\ell$ and $|J| = b\ell$. Thus the integral is given by

$$V = \pi b^2 \ell \int_{\bar{\eta}=0}^{\bar{\eta}=1} \int_{\bar{r}=\bar{\eta}-1}^{0} [\lambda(\bar{\epsilon}_r + \bar{\epsilon}_\theta + \bar{\epsilon}_\eta)^2 + 2\mu(\epsilon_r^2 + \epsilon_\theta^2 + \epsilon_\eta^2) + \mu\epsilon_{r\eta}^2] (1 + \bar{r}) dr d\eta \qquad (21)$$

where

$$\epsilon_r = \frac{\partial u}{\partial r} = \frac{\partial \bar{u}}{\partial \bar{r}}\frac{\partial \bar{r}}{\partial r} + \frac{\partial \bar{u}}{\partial \bar{\eta}}\frac{\partial \bar{\eta}}{\partial r} = \frac{1}{b}\frac{\partial \bar{u}}{\partial \bar{r}} + \frac{\partial \bar{u}}{\bar{\eta}_j} \equiv \bar{\epsilon}_r \tag{22}$$

$$\epsilon_\theta = u/r = \frac{\bar{u}}{b(1+\bar{r})} \equiv \bar{\epsilon}_\theta \tag{23}$$

$$\epsilon_\eta = \frac{\partial w}{\partial z} = \frac{\partial \bar{w}}{\partial \bar{r}}\frac{\partial \bar{r}}{\partial z} + \frac{\partial \bar{w}}{\partial \bar{\eta}}\frac{\partial \bar{\eta}}{\partial z} = -\frac{1}{l}\frac{\partial \bar{w}}{\partial \bar{\eta}} = \bar{\epsilon}_\eta \tag{24}$$

$$\epsilon_{r\eta} = \frac{\partial u}{\partial z} + \frac{\partial w}{\partial r} = -\frac{1}{l}\frac{\partial \bar{u}}{\partial \bar{\eta}} + \frac{1}{b}\left(\frac{\partial \bar{w}}{\partial \bar{r}} + \frac{\partial \bar{u}}{\partial \bar{\eta}}\right) \tag{25}$$

$$\bar{u} = a\bar{r}^2\bar{\eta}^2(1 + \bar{r} - \bar{\eta})^2$$

$$\bar{w} = -\frac{ab}{l}\bar{r}^2\bar{\eta}^2\left(\frac{1}{3}\bar{\eta} + \frac{1}{2}\bar{r}\right) .$$

In the following equations $\bar{r}$ and $\bar{\eta}$ are written without bars

$$\bar{\epsilon}_r = \frac{2ar\eta}{b}(1 + r - \eta)^2(r + \eta) \tag{26}$$

$$\bar{\epsilon}_\theta = \frac{ar^2\eta^2(1 + r - \eta)^2}{b(1 + r)} \tag{27}$$

$$\bar{\epsilon}_\eta = \frac{1}{l}\frac{ab}{l}r^2\eta(\eta + r) . \tag{28}$$

The expression for $\bar{T}$ in new variables is

$$\frac{T}{p^2} = \bar{T} = \rho\pi b^2 l \int_{\eta=0}^{\eta=1}\int_{r=\eta-1}^{0}(u^2 + w^2)(1 + r)dr d\eta . \tag{29}$$

The expression for V and $\bar{T}$ can be rewritten in by introducing the notation ϵ_r, ϵ_θ, ϵ_η, as

$$\frac{a}{b}\tilde{\epsilon}_r = \epsilon_r, \quad \frac{a}{b}\tilde{\epsilon}_\theta = \epsilon_\theta, \quad \frac{a}{b}\tilde{\epsilon}_\eta = \epsilon_\eta, \quad \frac{a}{b}\tilde{\epsilon}_{r\eta} = \epsilon_{r\eta} \qquad (30)$$

Then

$$V = \pi b^2 l \cdot \frac{a^2}{b^2} \int_{\eta=0}^{\eta=1} \int_{r=\eta-1}^{r=0} \left[\lambda(\tilde{\epsilon}_r + \tilde{\epsilon}_\theta + \tilde{\epsilon}_\eta)^2 + 2\mu(\tilde{\epsilon}_r^2 + \tilde{\epsilon}_\theta^2 + \tilde{\epsilon}_\eta^2) + \mu\tilde{\epsilon}_{r\eta}^2\right](1+r)\,dr\,d\eta \qquad (31)$$

Similarly, with the introduction of

$$a\tilde{w} = w$$
$$a\tilde{u} = u \qquad (32)$$

the expression for $\bar{T}$ becomes

$$\bar{T} = \rho\pi b^2 l a^2 \int_{\eta=0}^{\eta=1} \int_{r=\eta-1}^{0} (\tilde{u}^2 + \tilde{w}^2)(1+r)\,dr\,d\eta \qquad (33)$$

The quantity that needs to be computed is

$$p^2 = \frac{V}{\bar{T}}$$

If we let $E\tilde{\lambda} = \lambda$, $E\tilde{\mu} = \mu$

$$\nu = 0.3, \quad \tilde{\lambda} = \frac{\nu}{(1+2)(1-2\nu)}$$

and

$$\tilde{\mu} = \frac{1}{2(1+\nu)},$$

then

$$\frac{\rho b^2 p^2}{E} = \frac{\int_{\eta=0}^{\eta=1}\int_{r=\eta-1}^{r=0} [\tilde{\lambda}(\tilde{\epsilon}_r + \tilde{\epsilon}_\theta + \tilde{\epsilon}_\eta)^2 + 2\tilde{\mu}(\tilde{\epsilon}_r^2 + \tilde{\epsilon}_\theta^2 + \tilde{\epsilon}_\eta^2) + \tilde{\mu}\tilde{\epsilon}_{r\eta}^2](1+r)\,dr\,d\eta}{\int_{\eta=0}^{\eta=1}\int_{r=\eta-1}^{r=0} (\tilde{u}^2 + \tilde{w}^2)(1+r)\,dr\,d\eta} \qquad (34)$$

The integrals above are evaluated numerically by summing properly weighted values of the integrands at mesh points, the mesh being superimposed over the triangle in the preceding diagram (on page 24). In the example $b/l = 0.8928$ and $b/l = 0.4464$ were considered and the calculated values of p^2 are

$$p^2 = 33.88 \frac{Eb^2}{\rho l^4} \frac{b}{l} = 0.8928$$

and

$$p^2 = 1.1359 \frac{Eb^2}{\rho l^4} \frac{b}{l} = 0.4464 \quad .$$

These values do not give an estimate of the true values of p^2. More reliable results can be obtained by selecting more free parameters such as 'a' in equations (16) and (17), and establishing convergence numerically.

Furthermore, it should be noted that the results of the two-dimensional problem very much depend on the boundary conditions on the surface $z = 0$. The conditions existing in an experiment should be carefully designed before any accurate estimates can be done.

4. A Very Simple Approximation

The solution of complete two-dimensional problems is very difficult. However, in order to get accurate results we should attempt to solve the problem. In the meanwhile a very simple model has been constructed to get the order of magnitude of the frequencies.

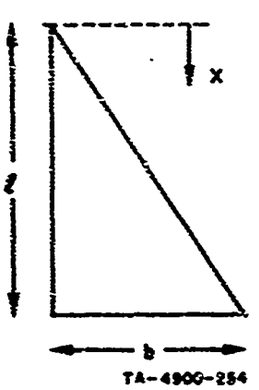

TA-4900-254

The cylinder is held together by shearing stresses τ_{rz} and normal stresses σ_θ. It will be assumed these are small and can be neglected. Then the cylinder under consideration can be considered to be consisting of infinite numbers of thin laminae of triangular shape. These laminae can vibrate independent of each other. Then the problem reduces to finding the natural frequency of vibration of a thin lamina of the following shape.

This lamina will be considered as a simple cantilever beam of varying cross-section.

Then the deflections y of the beam can be assumed to be

$$Y = X(x) \cos pt \quad .$$

The boundary conditions to be satisfied are

$$(1) \quad EI(x) \frac{d^2X}{dx^2} = 0 \qquad x = 0$$

$$(2) \quad \frac{d}{dx}\left[EI(x)\frac{d^2Y}{dx^2}\right] = 0 \qquad x = 0$$

$$(3) \quad X = 0 \qquad x = l$$

$$(4) \quad \frac{dX}{dx} = 0 \qquad x = l$$

The solution has been attempted by the Ritz method.

The following expression for X has been assumed.

$$X = a_1\left(1 - \frac{x}{l}\right)^2 + a_2 \frac{x}{l}\left(1 - \frac{x}{l}\right)^2 + \ldots .$$

This expression satisfies the boundary-condition. Then the Ritz method reduces to the evaluation of p by the following equation:

$$p^2 = \frac{E}{\rho} \frac{\int_0^l I(x) \left(\frac{d^2X}{dx^2}\right)^2 dx}{\int_0^l \frac{bx}{l} X^2 dx}$$

where

$$I(x) = \frac{1}{12}\left(\frac{bx}{l}\right)^3 .$$

With $a_2 = 0$, the evaluation of integrals yields

$$p^2 = \frac{10}{4} \frac{E}{\rho} \frac{\delta^2}{l4} .$$

If we use both a_1 and a_2 then we have to use Raleigh-Ritz method of minimizing the integral

$$S = \int_0^l \left[I(x) \left(\frac{d^2 X}{dx^2} \right)^2 - p^2 \frac{A\rho}{E} X^2 \right] dx \quad .$$

This process yields

$$p^2 = \frac{9.431}{4} \frac{E}{\rho} \frac{b^2}{l4} \quad .$$

The frequency f is given by

$$f = \frac{p}{2\pi} \quad .$$

III EXPERIMENTAL STUDIES

A. Studies of Particle Size and Velocity Distribution

1. Ultrasonic Disseminator

The ultrasonic disseminator used for these studies is similar to one described earlier.[5] The design followed quasi-optical principles for circular Fresnel lens construction, assuming that an ultrasonic beam reflects from an air-solid boundary following the same laws normally applied to light reflections. The disseminator is shown in cross-section in Figure 2 and constructed ready for operation in Figure 3. Construction is of solid aluminum, and the ultrasonic energy is supplied by

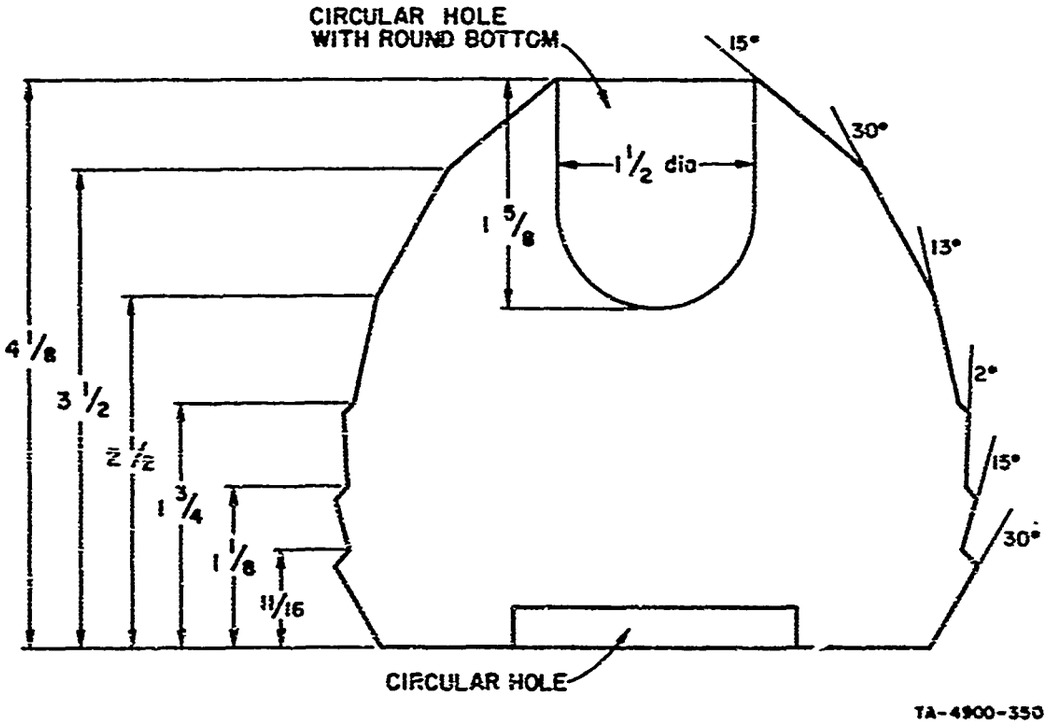

FIG. 2 CROSS-SECTIONAL VIEW OF THE ULTRASONIC DISSEMINATOR

FIG. 3 ULTRASONIC DISSEMINATOR WITH BONDED TRANSDUCER

a 2-inch-diameter, 1.25-inch-long, lead zirconate solid cylinder fitted in the circular hole in the base. Maximum vibration occurs on the upper conical face over a ring area adjacent to the lip of the center hold. Considerable vibration also occurs over much of the surface of the center hole, though it is of lower amplitude. For these studies, only the high amplitude area has been used. As constructed, the device is far from optimum: much basic information concerning the focusing of sound waves from a cylindrical source remains to be learned.

The electronic device used to drive the lead zirconate cylinder is a self-excited oscillator in which the transducer becomes a component in the output stage. By proper tuning, the driver can be made to "lock on" to the resonant frequency of the transducer-disseminator combination and deliver maximum power at that frequency. The actual circuit used (Figure 4) is an extensive modication of one used by Perron[6] to power an

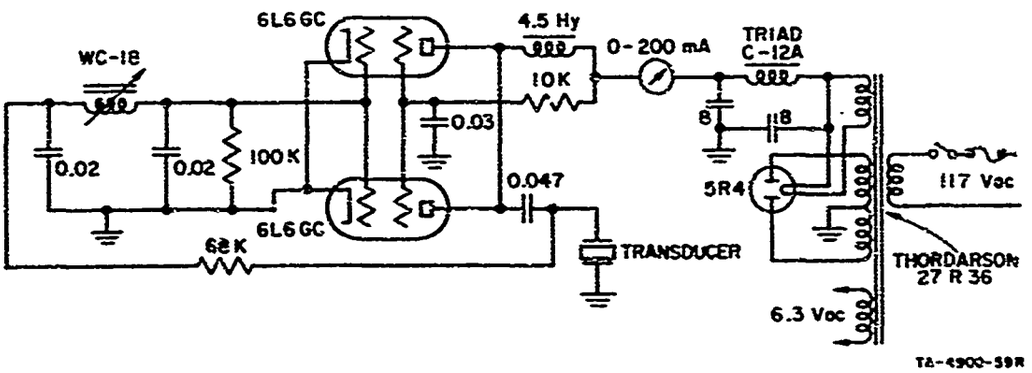

FIG. 4 SELF-EXCITED OSCILLATOR

ultrasonic oil burner. The use of a resonant device has provided a more stable drive to the disseminator and has proved much less bulky and troublesome to operate than the standard combination of RF oscillator and wide-band power amplifier.

2. Measurement Equipment and Techniques

A photo-optical technique was used to directly measure properties of the aerosol produced using the ultrasonic disseminator. The measurement system had to provide a method of enlarging the images of the

aerosol droplets to a usable size, a method of recording the images thus produced, and a method of lighting the images so that instantaneous velocity information from individual droplets could be recorded for later analysis. The chosen technique imposed a limitation on the size of the aerosol spray: it had to be confined to a narrow stream, so that individual droplets could be easily distinguished without being obscured by the many other droplets which would be present in a full circular spray. The disseminator operating in this manner is shown in Figure 5.

a. Optical Apparatus

The design of the optical system is shown in part in Figure 6 Light from the electronic flash unit is collimated before passing through the aerosol spray. Images of the aerosol droplets, which appear opaque when illuminated from the rear, are focused by the objective lens. A negative lens placed at this focal plane enlarges the image, producing a magnification of 26X at the final film plane. The film is mounted in a 4 × 5 view camera equipped with a shutter synchronized with the flash unit.

b. Electronic Flashtube Light Source

An electronic flash source was designed to provide short-duration light pulses for recording droplet images on film without noticeable movement. The unit was developed for two purposes: (1) to produce single-flash illumination of the aerosol stream for investigating the method of droplet formation at the surface of the disseminator and to investigate droplet size distribution at various locations in the aerosol stream; and (2) to produce double-flash illumination for studying droplet velocities in the stream.

This unit employs two flat-face, 3/4-inch-diameter flashtubes which have flash durations of 10 μsec, and a step-adjustable time delay between flashes of 20 μsec to 5 millisec. Figure 7 shows a schematic diagram of the unit as operating for use with high-speed black and white film. When color film was employed for studying the droplet velocities described below, the short flash durations fell within the film's reciprocity failure region, causing an apparent loss of film speed. For use with color film, the size of the storage capacitors was doubled.

FIG. 5 ULTRASONIC DISSEMINATOR WITH LIQUID-FEED ARRANGEMENT FOR PRODUCTION OF NARROW AEROSOL STREAM

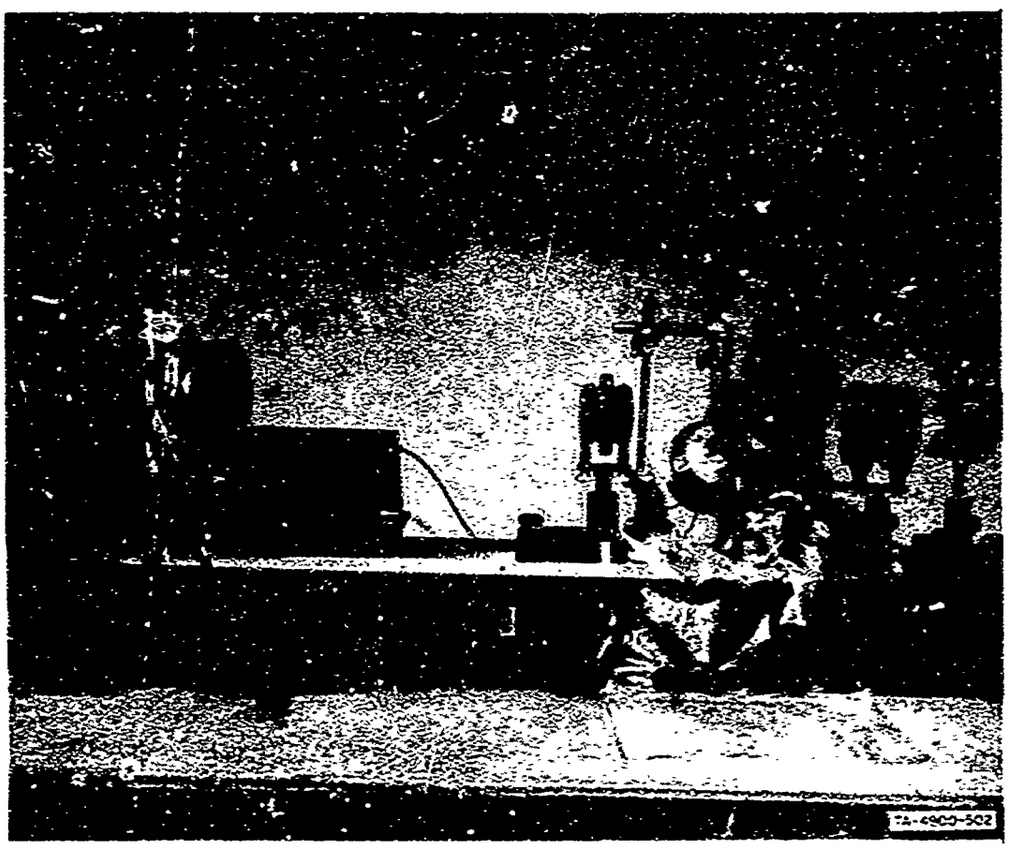

FIG. 6 OPTICAL APPARATUS WITH THE ULTRASONIC DISSEMINATOR IN PLACE AND OPERATING

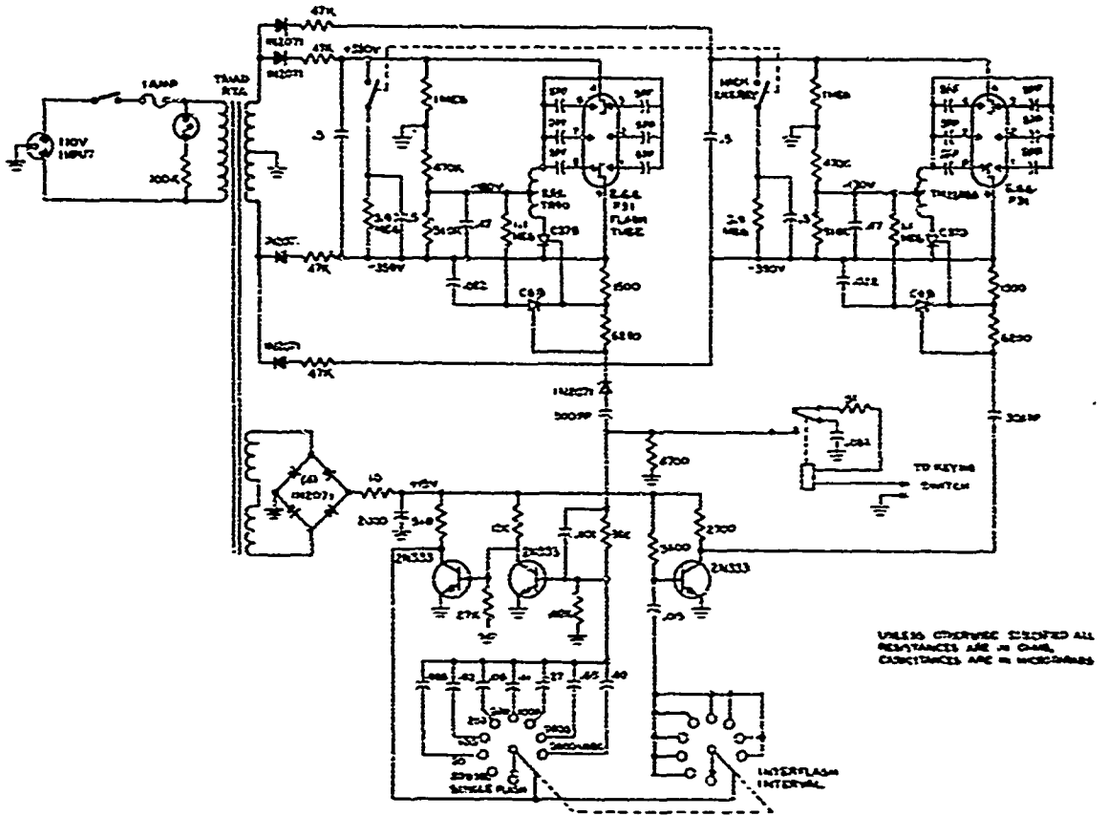

FIG. 7 DOUBLE-FLASH UNIT WITH VARIABLE FLASH INTERVAL

To focus both flashtubes at the point of droplet dissemination, a device resembling a beamsplitter was devised (Figure 8). With this arrangement, the light from one flashtube passes directly through a half-silvered mirror while the other is first reflected by a fully silvered mirror and then by a half-silvered mirror. Thus both light sources appear to be produced at the same point and can be accurately focused at the moving droplets.

c. Color Photography Technique

Studies of droplet velocities with the dual flash unit using two short-duration light flashes separated by a known interval were initially performed using black and white film as the recording medium, with typical results as in Figure 9. Two images of each droplet were recorded on the film and the distance of travel during a known interval could

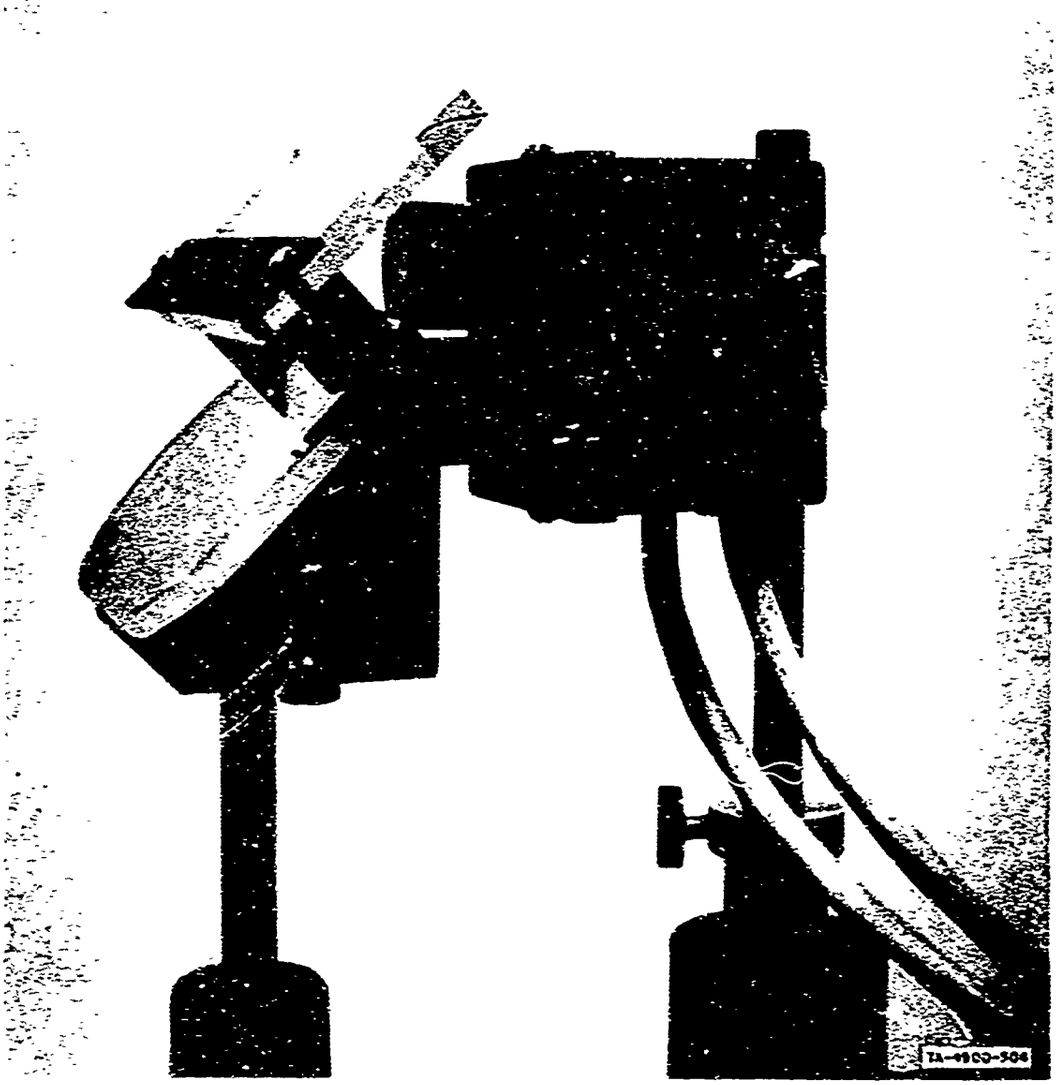

FIG. 8 DOUBLE-FLASH HEAD AND COMBINING MIRRORS

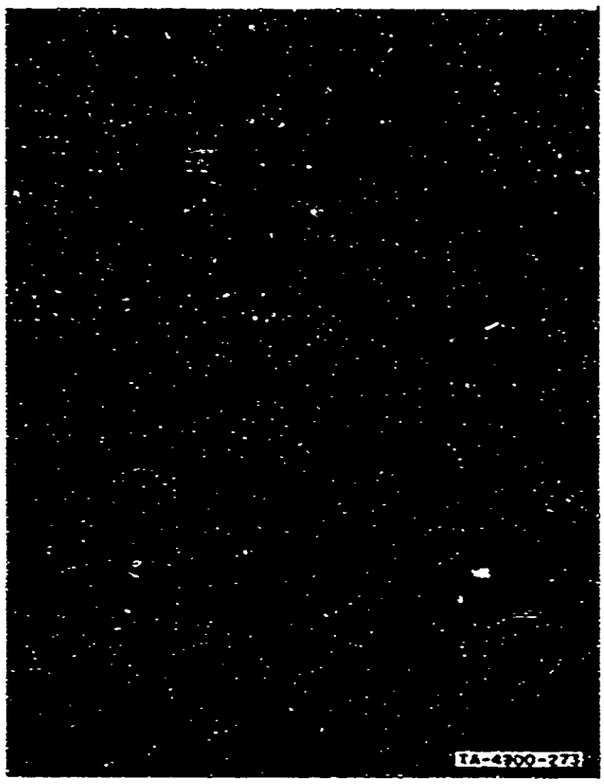

FIG. 9 DOUBLE-FLASH PHOTOGRAPH OF AEROSOL STREAM. Disseminator surface at lower left. Flash interval 200 μsec. Magnification 26X.

then be measured and the velocities of individual droplets calculated. Those photographs showed that it was possible—though often difficult—to identify many apparent droplet "pairs," i.e., the same droplet photographed by the two flashes. However, with so many droplets present, positive pair identification became tenuous, since droplet diameter was the only criterion for selecting pairs. For this reason, we investigated color techniques to aid in separating the droplet stream recorded by the first flash from the stream recorded by the second. With succeeding exposures of contrasting colors, correct pair identification could be accomplished more reliably and more often.

A color filter was placed over one of the flashtubes, the output of which then contrasted with the natural bluish output of the unfiltered tube. After experimentation with 10 colors, a light yellow No. 6(KI)

Wratten filter was chosen. Times ranging from 20 μsec to 5 msec between exposures were tried; a good time difference for positive droplet pair identification and accurate distance measurement is 200 μsec.

At the same time, we experimented with various color films in a search for a material that could produce an image with usable color contrast while retaining sufficient sensitivity with the short (10 μsec) exposure time and without objectionable gain size. Polaroid Type 58 color film was first tried as the recording medium but was soon abandoned because it did not have the necessary speed. The next material tried was Kodak Ektachrome sheet film, which produced marginally usable results when specially processed for 4X (2 stop) increase in effective film speed. This special processing, while affecting the color balance of the film (often nonreproducibly), did not materially increase grain size or reduce acuteness.

The search for a suitable recording medium ended after experimenting with roll-size Kodak High-Speed Ektachrome film. This film, which has a sensitivity advantage of 3X over Ektachrome, can produce usable results with normal processing methods.

An example of the results obtained using this technique is shown in Figure 10. Here, the first set of droplets is blue and the second set is yellow, with the background a combination of these colors. The exposure was made in the following manner. The first flash was through the yellow filter, exposing the film everywhere except through the aerosol droplets, the areas of which were left unexposed (opaque). The second and bluish flash occurred 200 μsec later, exposing the film everywhere except in the areas then occupied by the droplets. Thus, the background assumed a greenish color and the areas left unexposed by the first flash were exposed blue. The positions the droplets occupied during the blue flash were not exposed to the blue and were left yellow.

Many of the data for droplet size distribution studies were taken with this color film and single flash illumination. The droplet edge definition was superior to that obtained using fine-grained black and white film. In this case, one unfiltered flash was used, producing transparencies showing a blue background which contrasted well with the opaque droplets.

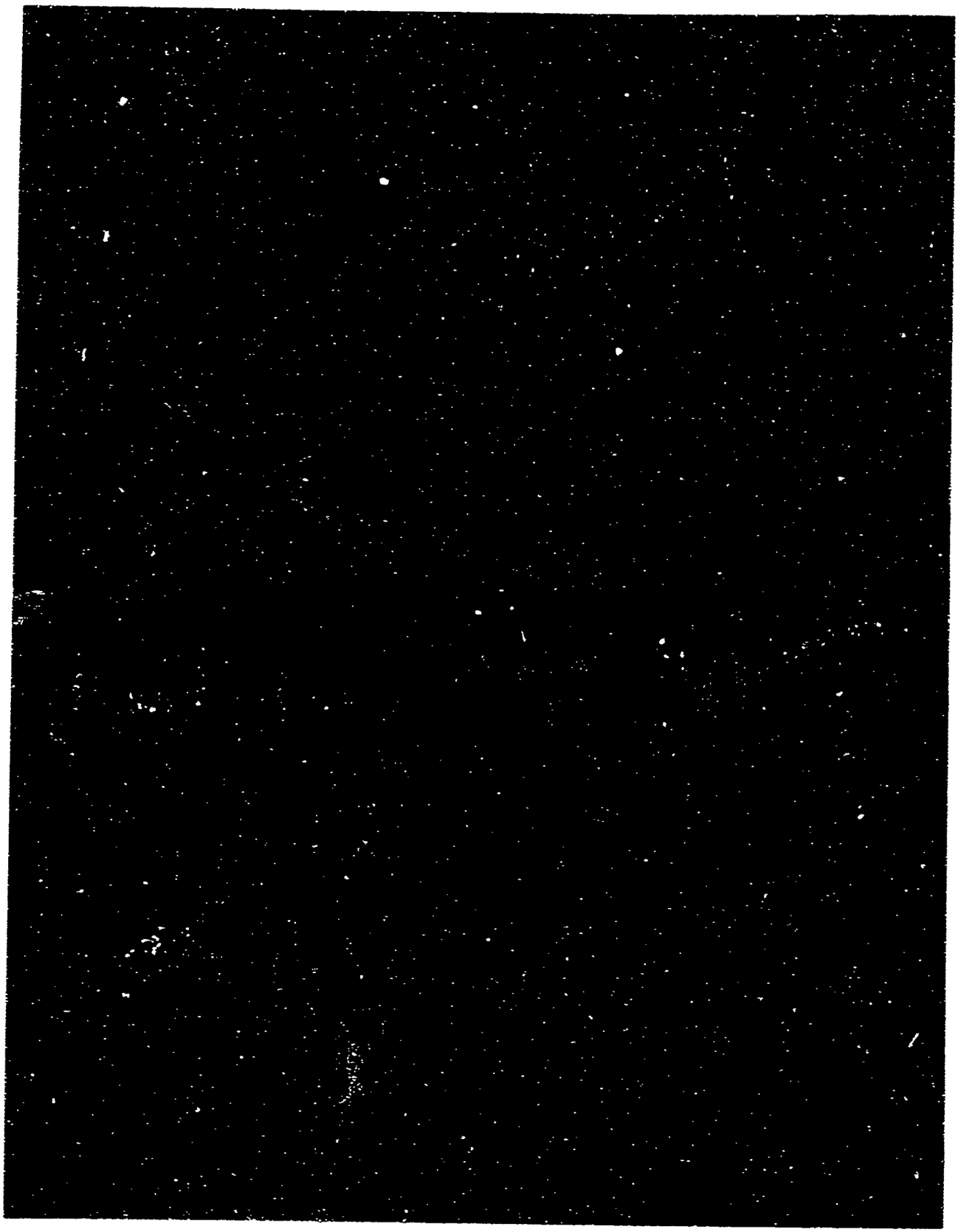

FIG. 10 DOUBLE-FLASH COLOR PHOTOGRAPH OF THE AEROSOL STREAM. Interval between flashes is 200 μsec. Droplets appear blue in the first position and yellow in the second position. A section of the disseminator surface appears in the lower left corner. Magnification 95X.

Readout of both droplet diameter and distance of travel was accomplished using a Tele-Readex Model No. 29E-32 film analyzer which permits 10X viewing of projected images and provides for first digital readout.

3. Data and Results

All data were taken while the disseminator was operating at resonance, about 53 kHz. Because the construction was imperfect, three or four individual resonances could be obtained using slightly different tuning settings of the self-excited oscillator. Changes in temperature during operation would also slowly shift the resonant frequency. During each experimental run, the device was constantly retuned, and care was taken to ensure that the same resonant peak was used for each complete run. Power delivered to the disseminator averaged 5.5 watts for all runs.

Test liquids were applied to the active area of the disseminator by flowing them through a 26-gage hypodermic needle. Liquid flow rate was measured by observing the level change in a burette; the rate was varied by means of the burette stopcock and by varying the liquid head.

a. Aerosol Droplet Size Distribution as Affected by Surface Tension and Viscosity

To gain basic information about the physics of aerosol production, we first investigated the possible influence of surface tension and viscosity on aerosol formation. Each of the liquids listed in Table II was disseminated by the apparatus described above.

Table II

LIQUIDS SELECTED FOR AEROSOL DROPLET SIZE DETERMINATION

LIQUID	DENSITY (g/cm^3)	SURFACE TENSION (dynes/cm)	VISCOSITY (cp)
Water	1.00	72.7	1.00
Acetone	0.79	23.7	0.328
Ethanol	0.79	22.3	1.20
Methylene chloride	1.34	50.2	0.449
Toluene	0.87	28.5	0.590
Ethyl acetate	0.90	23.9	0.455

These early experiments were done before development of the photographic system was completed. The 26X photographs were made on Polaroid film and droplet diameters were read using a hand lens. All droplets in a one-millimeter-square area centered at a distance of 1 millimeter from the disseminator surface were measured and each droplet size was determined to the nearest 10-micron diameter. The results, showing the percentage of each droplet diameter encountered and the total number of droplets counted for each sample, are shown in Table III.

Table III

AEROSOL DROPLET DIAMETERS

LIQUID	TOTAL NUMBER OF DROPLETS	PERCENTAGE OF DROPLET DIAMETERS					
		10μ	20μ	30μ	40μ	50μ	60μ
Water	195	5%	23%	43%	23%	5%	1%
Acetone	176	31	38	20	8	2	1
Ethanol	302	43	37	17	3	--	--
Methylene chloride	266	19	27	20	18	11	4
Toluene	297	36	35	22	5	2	--
Ethyl acetate	367	41	33	17	7	2	--

The aerosol droplet diameters of the test liquids showed marked differences. The results of this early study indicate that, in the area chosen for analysis the diameter of the aerosol droplets produced appears to be controlled by the surface tension of the liquid. Lower surface tension produces smaller droplets. The viscosity of the liquid does not appear to effect droplet diameter.

b. Effect of Flow Rate on Aerosol Production

The rate of liquid flow to the active disseminator face was varied to determine how the resulting aerosol might be affected. We were chiefly concerned that the thickness of the liquid layer might change and would influence the size of aerosol droplets formed. This larger size, in turn, could affect velocity of droplet travel. Measurement results indicated little effect of flow rate on either droplet diameter or velocity.

For these experiments, distilled water was introduced to the active disseminator area and aerosolized as previously described. At each selected flow rate, single-flash photographs for droplet size measurements

and double-flash photographs for droplet velocity measurements were made in quick succession. In addition, tuning was carefully adjusted between each flow setting to minimize changes in the disseminator performance. Table IV indicates the results of analysis of the data photographs. As before, an area one millimeter square centered at a distance of one millimeter from the active face was investigated. For droplet size data, all in-focus droplets were counted. For droplet velocity, all in-focus, positively identified (by diameter and color) droplet pairs were measured.

Table IV

AEROSOL VELOCITY AND DROP SIZE DISTRIBUTION
AS A FUNCTION OF LIQUID FLOW RATE

FLOW RATE (ml/hr)	AV. DROPLET VELOCITY (mm/sec)	AV. DEVIATION (mm/sec)	NO. OF DROPLET PAIRS MEASURED	AV. DROPLET DIAMETER (microns)	NO. OF DROPLETS MEASURED
165	377	93	18	28.4	49
125	227	98	20	29.1	35
90	220	62	22	28.8	28
60	278	89	13	31.3	42
40	226	124	18	32	40
27	179	69	40	27.3	78

Except for a higher apparent average velocity noted at the highest (165 ml/hr) flow rate, there appears to be no definite change in average aerosol droplet velocity with flow rate change. At the highest flow rate, many of the droplet pairs were obscured by others and the result is less reliable. The reading was included to indicate the maximum flow rates that can be handled by the photographic technique. Average droplet diameter also appears not to be affected by changes in flow rates.

The narrow aerosol stream used for these measurements was necessary for the photographic technique. For actual operation, the disseminator would support flows of considerably higher rates, since liquid would be flowed onto the complete active area. Pending actual trials at full flows, we estimate that a rate of 100 ml/hr would correspond to a flow rate of between 5 and 8 liters/hr, if liquid were introduced over the entire active area.

c. Aerosol Stream at Distances from the Production Area

Some evidence pointing to droplet coalescence occurring at a distance from the disseminator had been noted in earlier experiments. It was thought that coalescence could accompany, or be caused by, reduction in the velocity of the droplet stream. Accordingly experimental data were taken of aerosol droplet sizes and velocities at distances of 1 to 40 mm from the disseminator. As before, droplets contained in a one-millimeter-square area about the nominal measurement point were analyzed. The liquid measured was again distilled water, and the driving frequency of the disseminator was 53 kHz. The liquid flow onto the active face was kept constant at 54 ml/hour for all measurements. The results of this series of measurements are shown in Table V.

Table V

AEROSOL DROPLET SIZE AND VELOCITY VERSUS DISTANCE FROM THE ACTIVE FACE

DISTANCE FROM ACTIVE FACE (mm)	AVERAGE DROPLET VELOCITY (mm/sec)	AVERAGE DEVIATION VELOCITY (mm/sec)	NUMBER OF DROPLET PAIRS MEASURED	AVERAGE DROPLET DIAMETER (microns)	NUMBER OF DROPLETS MEASURED
1	135	46.2	31	32.5	42
10	455	95	38	35.0	34
20	436	43	51	32.9	27
30	460	35.3	28	37.0	37
40	465	36.8	29	37.6	23

These measurements showed a very rapid increase in droplet velocity to a remarkably constant velocity at a distance of 1 to 10 mm from the disseminator. We have no definite explanation for this unexpected effect. There is a possibility that the observed effect was caused by an entrained airstream. When a continuous aerosol stream is generated, an airflow pattern is produced around and within the stream with a direction of travel parallel to the stream. It is therefore possible that such an airstream, once started, could positively affect the droplets away from the disseminator while having less effect, or even a negative effect, on droplets only one millimeter from the face. Another possible explanation is that the ultrasonic field generated in the air by the disseminator is acting on the water droplets. This type of effect was shown to exist in earlier work when aluminum particles were dispersed by the same type of

disseminator, and the effects of the ultrasonic field could be clearly seen on the suspended particles.[5] Both possible reasons for the velocity effect measured are only suppositions, and additional measurements will be necessary before definite answers can be given.

Droplet size distribution data showed that while some coalescence occurred as distance from the disseminator face increased, the percentage of small droplets remained high, actually increasing at some distances. The interaction of these two effects kept the average droplet size relatively constant as a function of distance. It should be noted that this is a rather insensitive way of determining coalescence, for the diameter increases only as the cube root of the volume; thus many coalescing drops are required to change the diameter of a droplet significantly. A clearer picture of the droplet size distribution can be obtained using the histograms in Figure 11. We think that evaporation may be playing a major role in the continued presence of many small droplets at distance and that an experiment using a high-vapor-pressure liquid should be run to investigate further the effect of distance on aerosol particle size distribution. Coalescence into larger drops would occur more often in operation when the whole active surface of a device is used. The geometrical spreading of the thin aerosol stream we used increased average drop separation. The average deviations in the velocity reported in Table V show that collision and coalescence are likely to occur.

4. High Flow-Rate Devices

Work previously performed on this contract produced a number of high flow-rate devices. The most successful one has been described elsewhere.[7] Briefly, the vibrating device consists of a ceramic piezoelectric disk bonded to a resonant metal wedge. Figure 12 shows the device in longitudinal cross-section. The mode of vibration of the ceramic transducer produces a type of "rocking" of the circular wedge. The outside of the vibrating wedge is surrounded by a metal ring that feeds liquid to the vibrating surface through many circumferential holes. Since the design procedures for this device were somewhat empirical, an attempt was made to obtain some design data from analysis. The circular wedge was first considered as consisting of thin, independent lamina, in the shape of the cross-section

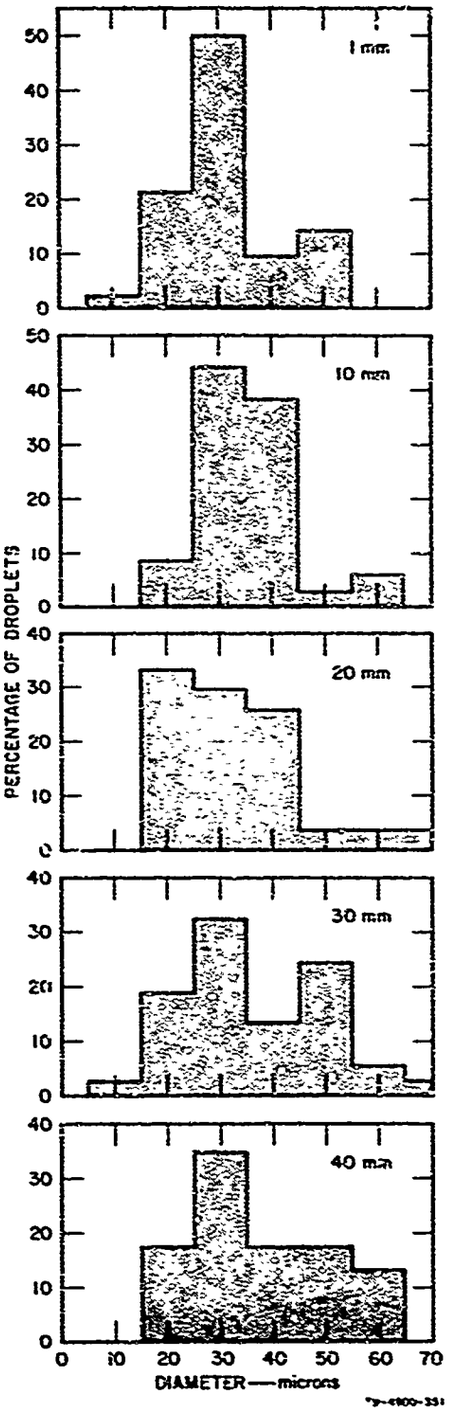

FIG. 11 HISTOGRAMS SHOWING DROPLET SIZE DISTRIBUTIONS AS A FUNCTION OF DISTANCE FROM THE DISSEMINATOR SURFACE

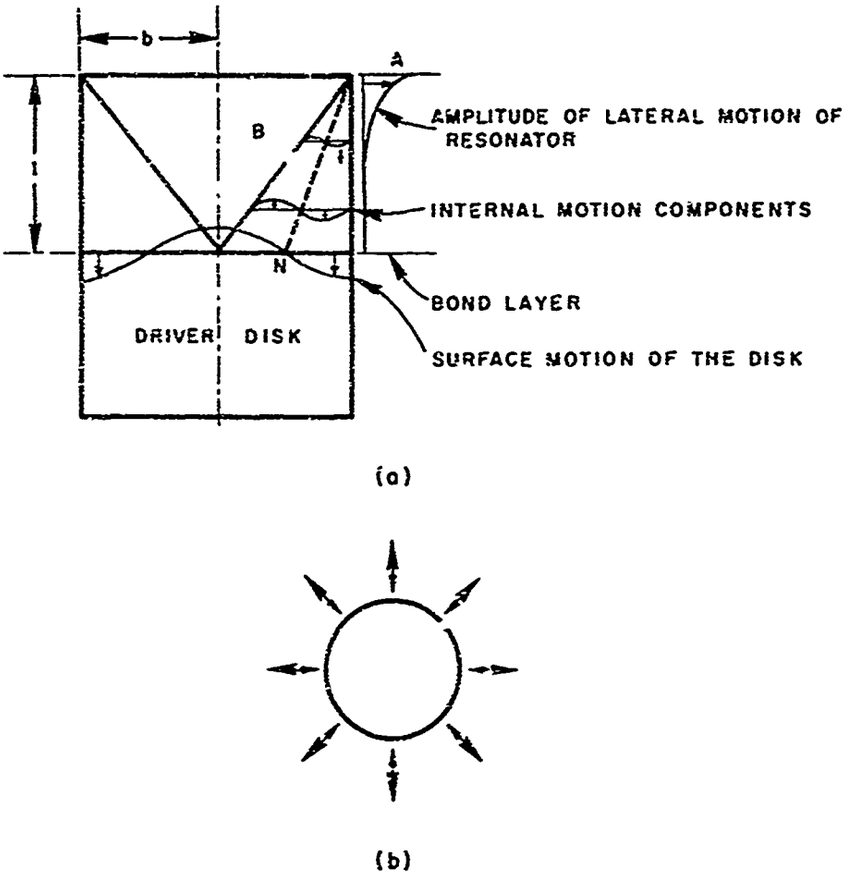

FIG. 12 VIBRATION OF THE CIRCULAR WEDGE ATOMIZER

shown in Figure 12. The resonant frequency of the lamina, treating the pointed end as being free and the other fixed, is given by

$$\omega^2 = \frac{9.431}{\rho} \frac{E}{\rho} \frac{b^2}{l^4} .$$

Here ω is the circular frequency, E is the modulus of elasticity, ρ is the density, b and l are the base (i.e. radius of the circular wedge) and length respectively. The existing wedge devices were examined for resonances in the frequency range predicted by this formula. Negative results suggested that the assumed thin lamina model was too simple, that is, one cannot ignore hoop-like vibration of the upper edge of the wedge. Analytical work was then pursued in which the vibration of the entire wedge was

considered. This work is described in Section II-B; time did not allow an experimental check of the analysis.

Since photographic techniques for obtaining droplet size distributions are not useful at high flow rates, a standard sampling technique was adopted for use with these devices. Briefly, a microscope slide covered with a thick layer of magnesi oxide was passed through the aerosol and the resulting "holes" in the powder layer were viewed with a microscope. The numerous problems with this technique have been described at length in the monthly and quarterly reports and will not be repeated here. At lower flow rates, the aerosol was sampled by this procedure and photographed by the technique described in the previous section. Number versus diameter distributions obtained by the two techniques show the photographic technique to yield sharper distributions of droplet sizes.

It was later suggested that the magnesium oxide technique is poor for this size range (40-50μ droplets from the 25 kHz-sec device) because the sizes of the "holes" are not only a function of the droplet size but also depend on the nature of the impact. It is also known that small droplets (say about 5μ in diameter) would tend to go around the slide. The suggested alternative procedure involved a Stokes law type of precipitation of droplets. One could utilize a simple vertical settling of the droplets or trap the aerosol in a horizontal laminar flow of air, from which the droplets would gradually settle out.

B. Studies of Capillary Waves and Aerosols

1. Step-Horn and Associated Equipment

The step-horn generator used in the observation of capillary waves and aerosols is shown in Figure 13. It consists of an aluminum, mechanical velocity-transformer bonded onto a PZT-4 ceramic transducer. This device is driven at 26 kHz/sec by a power amplifier built at SRI. With the inch-diameter active end horizontal, capillary waves were observed and photographed on this surface. A model VX-IIa Exakta camera was used, with extension tubes for the low magnification photos and with a microscope for the higher magnification photos. Aerosol production was usually studied with the emitting face vertical. The water aerosol thus neither coats the optics of our observing devices nor shorts the ceramic

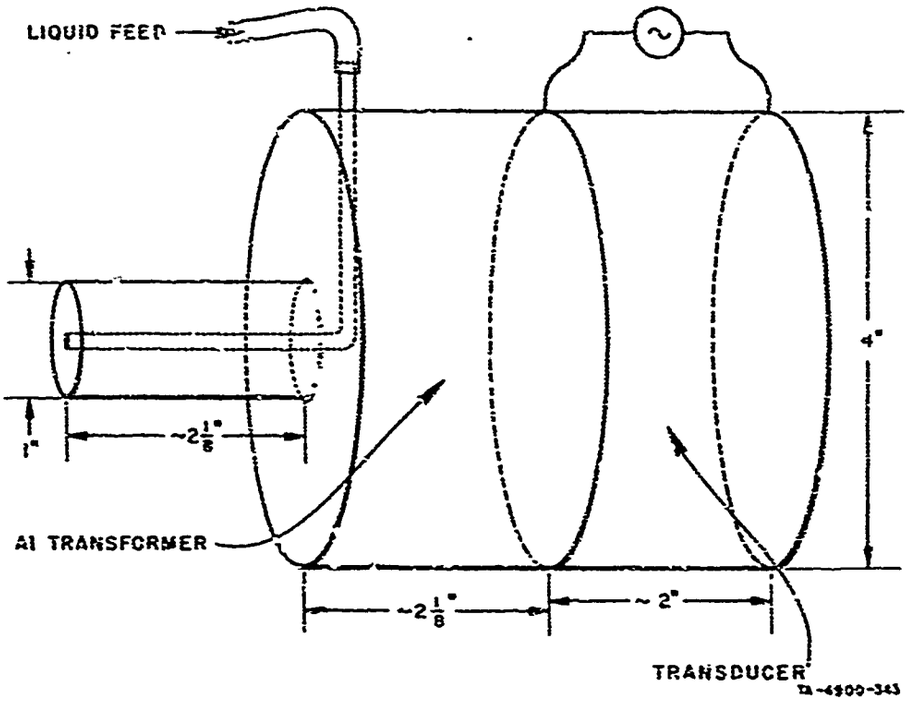

FIG. 13 STEP-HORN GENERATOR

transducer. In this arrangement the central hole is used to feed the liquid onto the active surface.

The amplitude of the mechanical vibration of the active tip of the step-horn assembly was measured with a model K-D45 Fotonic Sensor made by Mechanical Technology Inc. In this device, two bundles of optical fibers are used in conjunction with a light source and a photodiode. Light transmitted from the source by one bundle of optical fibers is incident on the vibrating surface. The reflected light, modulated by the vibrating surface, travels to a photodiode by the other bundle of optical fibers. Thus, the device has the advantage that it does not "load" the vibrating object to any appreciable degree. The main disadvantage of the Fotonic Sensor is that one cannot scan across a surface and obtain relative information.

2. Observations

If a small quantity of water is placed on a vibrating surface, and the excitation amplitude is varied, a number of stages through which the liquid passes can be observed with low-power magnification. Starting with a low initial amplitude and increasing it slowly, one first notices that although the liquid surface remains highly reflective, dust particles are moving on this surface, and tiny bubbles are moving around in the fluid. The next stage is characterized by more violent motion of these particles and generation of tiny air bubbles from rough places in the device surface. With more excitation, capillary waves appear around the edges of the liquid, accompanied by a partial loss of reflectivity. These capillary waves appear as fine lines running approximately perpendicular to the periphery of the liquid.

The photograph in Figure 14 shows the ridged vibrating device surface with liquid on the left side of the photograph. A separate drop of water appears in the center. With more excitation these capillary wave lines extend well into the major portion of the liquid surface (Figure 15a), and then the lines show evidence of breakup (Figure 15b). When the breakup is complete (Figure 16), one sees the dot-like patterns that are called crossed capillary waves. Viewing the liquid surface without magnification, one sees a general agitation of the surface and a major loss of reflectivity.

FIG. 14 CAPILLARY WAVES ON EDGE OF LIQUID FILM

FIG. 15(e) CAPILLARY WAVES

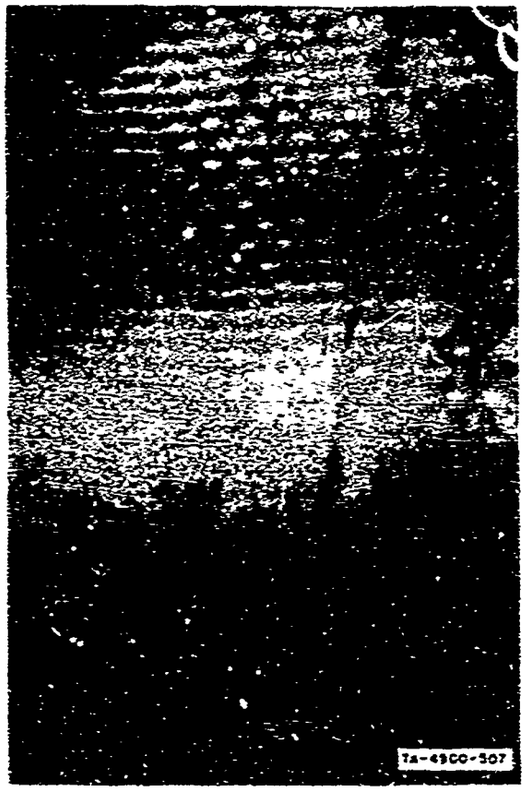

FIG. 15(b) CAPILLARY WAVES

FIG. 16 CROSSED CAPILLARY WAVES
(f = 26 kHz, amp 2.5×10^{-4} cm,
magnification 50X)

In the next stage of increased amplitude there are one or two slightly raised peaks from which aerosol is gently spewing, and the surface has taken on the appearance of frosted glass. The final stage is characterized by aerosol emanating from most of the surface and, consequently, a rapid loss of the liquid. Some minor hissing sounds are also associated with the process, but these may be partly due to the transducer itself.

a. Capillary Waves

The existence and nature of capillary waves is well described in the works of Benjamin and Ursell[2] and of Eisenmenger.[1] The governing equation has the form of Mathieu's equation

$$\frac{d^2V}{dt^2} + (p - 2q \cos 2t)V = 0 \quad . \tag{1}$$

V is the amplitude of the capillary wave, and p and q are parameters given by

$$p = \frac{4k^3T}{\rho\omega^2} \tanh kh \quad , \tag{2}$$

$$q = 2kA \tanh kh \quad ,$$

where

$$k = \pi^2(a^{-2} + b^{-2}) \quad . \tag{3}$$

The a and b are the dimensions of the waves in the two perpendicular directions lying in the plane of the liquid surface. The other parameters are given as follows: T is the surface tension, ω is the angular excitation frequency, h is the thickness of the liquid layer, and A is the excitation amplitude of vibration of the base. Solutions of Mathieu's equation are shown in Figure 17 in terms of the parameters p and q. The hatched areas are the regions of the unstable solutions that control capillary waves. Eisenmenger included a viscosity term in the governing equation that explains the capillary-wave threshold. Its effect on the unstable solutions of Mathieu's equation is to truncate the unstable zones—thus leaving the crossed-hatched areas in Figure 17 (the specific areas shown are for the case in which the liquid is water at room temperature). Mathematical details of these solutions are described at length in books by McLachlan[8] and Hayashi,[9] the former showing the effect of including the extra damping term. The theoretical and experimental work of Benjamin and Ursell in the cycle per second frequency region and by Eisenmenger in the kilocycle to megacycle per second region explains, in general, the nature of capillary waves. Eisenmenger has used the measurement of capillary wavelength to determine the surface tension of various surface-active agents.

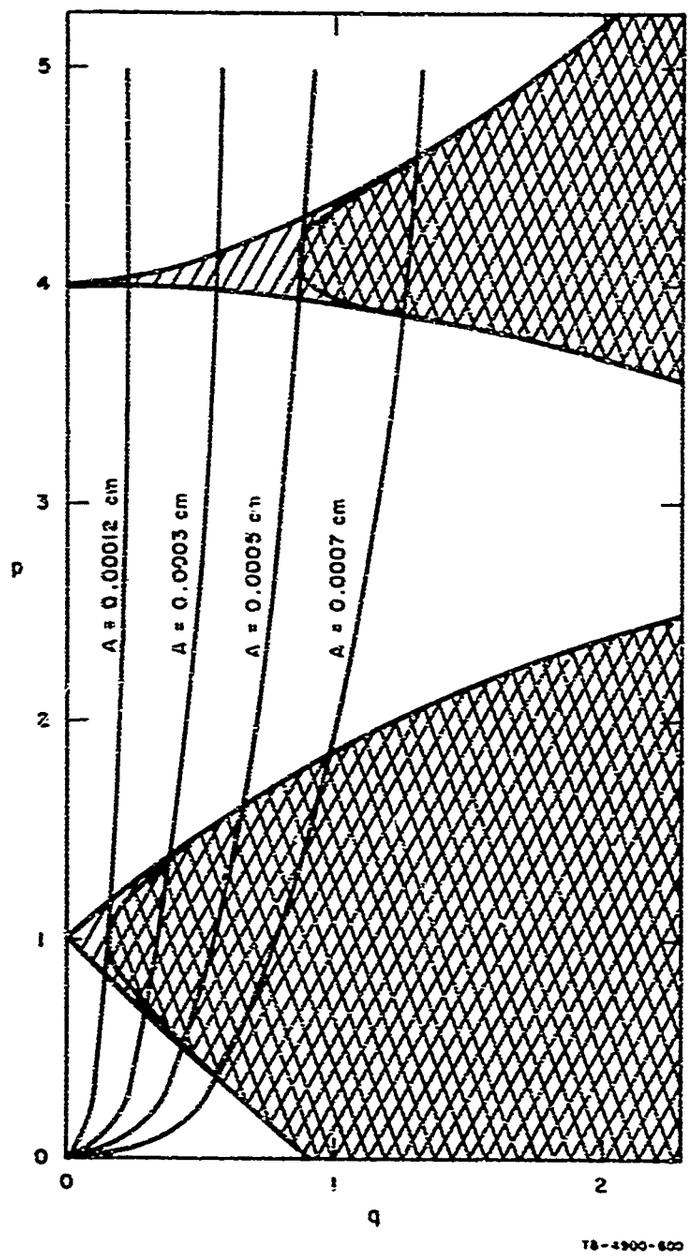

FIG. 17 SOLUTION ZONES OF MATHIEU'S EQUATION

The only mention of aerosol in these references is a statement by Eisenmenger that an aerosol is produced at a vibration amplitude of approximately four times the amplitude necessary for the formation of capillary waves. If one assumes that kh in (2) and (3) is greater than three (and rough measurements and calculations show that for our case it was), then the hyperbolic tangent terms may be set to unity. Minor manipulation then allows k to be eliminated from (2) and (3) and the following relation between p and q to be written in terms of known parameters.

$$p = \frac{4T}{\rho\omega^2} \frac{q^3}{A^3} \quad . \tag{4}$$

For water and an exciting frequency of 25 kHz/sec, p versus q curves have been calculated for various values of A, the vibration amplitude. These are the curves in Figure 17 that pass through the origin. Thus, for this specific case, one can see that a vibration amplitude of $A = 0.00012$ cm is necessary for the formation of capillary waves.

Measurement with a noncontacting optical probe (MTI, Fotonic Sensor, Model KD45) of the vibrational amplitude showed approximate agreement with the capillary-wave threshold predicted by Eisenmenger. Measurements of the threshold of aerosol production also seemed to agree with his claim of four times the vibration amplitude necessary for the capillary wave production. This is the $A = 0.0005$ cm curve in Figure 17. What has been noted and what is believed to be of major significance is that the p versus q line for an amplitude of four times the capillary-wave threshold just intersects the truncated second unstable region. Thus, at the inception of aerosol production one is just starting to excite the second unstable zone.

A calculation of the wavelength in the second region shows that it is related to the wavelength in the first region by:

$$\lambda_2 = 4^{-1/3}\lambda_1 \quad . \tag{5}$$

It is suggested then that this additional nonintegrally-related wavelength causes the disruption of the capillary waves and is instrumental in producing aerosol.

Measurements of thresholds of capillary wave formation and of aerosol production are subject to some variation. One source of this variation seems to be the presence of bubbles. Bubbles on the order of 0.25 mm to 0.5 mm in diameter move around in the thin liquid layer and they may initiate the formation of capillary waves and the production of aerosols, possibly before the predicted thresholds are reached. Bubbles appear from rough areas in the vibrating surface or from a deep scratch.

b. Cavitation

Cavitation has also been claimed as a basic mechanism in the formation of an aerosol. In this process, the generation and collapse of bubbles under intense sonic forces cause a disruption of the liquid surface. One sees evidence of cavitation in the atomization process. A polished aluminum vibrating surface from which aerosol has been produced shows evidence of cavitation damage. The surface takes on a "mottled" appearance that, with magnification, appears as numerous small irregular pits. One can also perform a standard test for cavitation, although an exact definition of cavitation is somewhat nebulous. The test consists of looking for the presence of chlorine in the atomization of a solution of carbon tetrachloride and water. The action of cavitation is to liberate the chlorine. Its presence is detected by a potassium-iodide test paper. The test indicated cavitation for our stepped-horn device.

Other liquids react differently under the influence of the vibrating surface. An extreme contrast to water is supplied by castor oil. Its surface tension is roughly half that of water and its viscosity is about one thousand times greater. With castor oil, one sees no evidence of capillary waves. Tiny bubbles move around in the thin layer, accompanied by a hissing sound—a characteristic of cavitation. At fairly high excitation one sees a fuzzy central bubble with numerous branches and subbranches (Figure 18). The central bubble also takes on a sickly yellow color. With the maximum amount of excitation presently available, no production of aerosol was noticed. With larger excitation, it is expected that atomization would occur, and it appears from the above description that cavitation would be the basic mechanism. Because of

FIG. 18 CASTOR OIL UNDER INTENSE VIBRATION
(f = 26 kHz, amp not noted, magnification 7X)

the high viscosity—and high capillary wave threshold—one expects cavitation disruption would occur in this liquid well below the capillary wave threshold. This may be part of the key to the relative importance of capillary wave disruption versus cavitation disruption—that is, if one reaches the capillary wave threshold, controlled by viscosity, before attaining the cavitation threshold, then the capillary wave phenomenon will be the controlling mechanism. The converse situation would then hold if the viscosity was sufficiently high.

The appearance is different when water is atomized at measurable flow rates. Instead of the fairly thick (i.e., surface tension control) "puddle" one finds a fairly thin layer on the vibrating surface of the step-horn. This surface and the emitted aerosol are shown in Figures 19 and 20. Crude measurements of this layer show it to be about 0.25 mm thick. Over the range of flow rates of 2 to 50 ml/min, this layer maintains approximately the same thickness with only the wetted area of the horn tip (vibrating surface) varying.

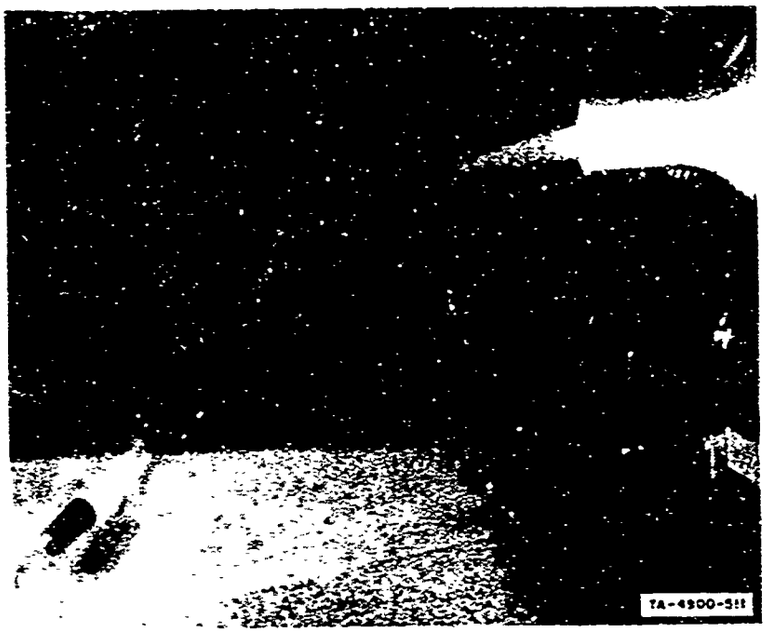

FIG. 19 STEP-HORN AND AEROSOL

FIG. 20 CLOSE VIEW OF AEROSOL AND STEP-HORN

IV SUMMARY AND CONCLUSIONS

The theory of incompressible, inviscid fluid flow was applied to find the wavelength and stability of capillary waves in a thin liquid layer over an oscillating reed. Results of this analysis showed that waves of amplitude comparable to that of the reed tip oscillation are excited by simple resonance rather than by the parametric excitation that initiates very small capillary waves. This implies that surface wave forms will be simple sinusoids. Assuming that the instability of these waves is a major mechanism for aerosol formation, droplet sizes at formation should be quite uniform. A second result is that pressure extremes occur at the free surface, where they are balanced by inertial forces and surface tension. In this theory, internal tensile maxima for cavity formation arise near the free surface of the liquid.

An open question for theoretical and experimental study is a determination of the boundaries between the parametric and the resonant capillary wave regimes. Examination of the real fluid effects of viscosity and compressibility and observation of surface wave forms as a test of the theoretical considerations are also needed.

An apparatus for the dissemination of aerosols has been described. A photo-optical technique has been devised and perfected for measuring velocity and size of aerosol droplets. The preliminary results of this work lead to the following conclusions:

1. Surface tension appears to be a controlling factor in the size distribution for the liquids examined.
2. Rate of flow fo. distilled water in the range of flow rates examined has a secondary effect on size and velocity distributions.
3. Sampling of droplet size and velocity at varying distances shows a remarkable uniformity after the close-in sample.

This work is necessarily incomplete; one cannot claim to understand aerosol generation from the high-flow devices on the basis of these results. The effect of different frequencies and the role of liquid evaporation must be examined.

The various stages of the excitation of a thin layer of liquid have been examined and described. The theory of capillary waves is reasonably well established, but the transition to aerosol still rests on an empirical basis. A possible explanation has been suggested for this transition. It has been shown that cavitation plays a role in the production of aerosol, and that the relative balance between cavitation and capillary waves as aerosol generating mechanisms is probably governed by the viscosity of the liquid. The governing mechanism is determined by whether the liquid reaches the cavitation threshold before attaining the capillary wave threshold and its subsequent aerosol threshold. Further work should examine liquids of varying viscosity to check the proposed hypothesis.

V EVALUATION AND RECOMMENDATIONS

Work on sonic generation of aerosols was terminated before any significant advances were made in understanding the physical process. Much of the experimental effort described in this report was directed toward the development of the theoretical and experimental tools needed in our study. These tools should be useful in any future study of sonic aerosol generation.

Among the preliminary results was a determination of particle size in aerosols produced by one of our high flow-rate devices. Less than 1 percent of the liquid mass was in the drops with diameters less than 10 microns. Drop sizes could be reduced by lowering the surface tension of the liquid or by raising the operating frequency of the device. We do not know how easily surface tensions of agents may be varied. The operating frequency of the wedge device in Figure 12 may most easily be raised by making the device smaller. However, this change would also reduce the flow rate.

Sonic aerosol generators could be useful in chemical weapons research in the following ways:

1. Clandestine dissemination of agents.
2. Harmless dissemination of incapacitating agents.
3. Laboratory tool for study of aerosols with controlled drop sizes.
4. Dissemination of delicate chemical or biological agents that would be rendered ineffective by explosive dissemination.

REFERENCES

1. Eisenmenger, W., "Dynamic Properties of the Surface Tension of Water and Aqueous Solutions of Surface-Active Agents with Standing Capillary Waves in the Frequency Range from 10 kc/sec to 1.5 Mc sec," Acustica 9, 327 (1959).

2. Benjamin, T. B., and F. Ursell, "Stability of the Plane Free Surface of a Liquid in Vertical Periodic Motion," Proceedings of the Royal Society, London, Vol. A225, pp 505-515 (1954).

3. Peskin, R. L., and R. J. Raco, "Ultrasonic Atomization of Liquids" Journal of the Acoustical Society of America, Vol. 35, pp 1378-1381 (1963).

4. Lamb, H., *Hydrodynamics*, 6th Ed. Dover Publ. Co., New York, 1945.

5. Poppoff, I. G., "Research Studies on the Dissemination of Solid and Liquid Agents," Fourth Quarterly Progress Report, Stanford Research Institute, March 25, 1965.

6. Perron, R. R., J. R. Swanton, and E. S. Shanley, "A Practical Ultrasonic Oil Burner," Conference Paper CP 63-1, 1963 American Petroleum Institute Conference on Distillate Fuel Coebustion, Chicago, Illinois.

7. Martner, J., "An Ultrasonic Atomizer Capable of High Rates," 1966 API Research Conference on Distillate Fuel Combustion.

8. McLachlan, N. W., *Theory and Application of Mathieu Functions*, Oxford University Press, London, 1951.

9. Hayashi, C., *Forced Oscillations in Nonlinear Systems*, Nippon Printing and Publishing Co., Osaka, Japan, 1953.

UNCLASSIFIED

Security Classification

DOCUMENT CONTROL DATA - R & D

(Security classification of title, body of abstract and indexing annotation must be entered when the overall report is classified)

1. ORIGINATING ACTIVITY (Corporate author)	2a. REPORT SECURITY CLASSIFICATION
Stanford Research Institute Menlo Park, California 94301	UNCLASSIFIED
	2b. GROUP N/A

3. REPORT TITLE

ULTRASONIC DISSEMINATION OF AEROSOLS

4. DESCRIPTIVE NOTES (Type of report and inclusive dates)

Special Report

5. AUTHOR(S) (First name, middle initial, last name)

Smith, C. W., Ablow, C. M., Hanagud, S. V., Spurlock, B. M., and Grine, D. R.

6. REPORT DATE	7a. TOTAL NO. OF PAGES	7b. NO. OF REFS
July 1967	72	9

8a. CONTRACT OR GRANT NO.	9a. ORIGINATOR'S REPORT NUMBER(S)
DA-18-035-AMC-122(A) b. PROJECT NO.	SRI Technical Report No. 9
c. TASK 1B522301A08101	9b. OTHER REPORT NO(S) (Any other numbers that may be assigned this report) N/A
d.	

10. DISTRIBUTION STATEMENT This document is subject to special export controls and each transmittal to foreign governments or foreign nationals may be made only with prior approval of the CO, Edgewood Arsenal, Attn: SMUEA-TSTI-T, Edgewood Arsenal, Maryland 21010.

11. SUPPLEMENTARY NOTES	12. SPONSORING MILITARY ACTIVITY
Dissemination investigations of liquid and solid agents	Physical Research Laboratory Research Laboratories Edgewood Arsenal, Maryland 21010

13. ABSTRACT

An investigation of the generation of aerosol by ultrasonic means was started. Although the work was terminated before it could be completed, the methods and results of this report should be useful in any future study. The theory of a liquid flow over the surface of an oscillating reed was studied to help the understanding of high flow-rate devices. A simple resonance theory has been developed which contrasts with the usual parametric capillary wave theory. An experimental photo-optical technique has been devised and used to give quantitative information on droplet size and velocity distributions. Capillary wave behavior has been examined experimentally and compared with existing theory. A possible explanation of the transition of capillary waves to an aerosol has been suggested. The existence of cavitation during sonic aerosol production from water was verified.

14. KEYWORDS

Aerosols	Solids
Dissemination	Photo-optical
Ultrasonic	Technique
Particle size	Flow rate
Device	Reed
Model	Mathematical model
Liquids	Cavitation

DD FORM 1 NOV 65 1473 (PAGE 1)

S/N 0101-807-6801

UNCLASSIFIED

Security Classification